# Numerical study of high-Ra Rayleigh-Bénard mercury and water convection in confined enclosures using a hybrid RANS/LES technique

A.G. Abramov, N.G. Ivanov and E.M. Smirnov
*Department of Aerodynamics, Saint-Petersburg State Polytechnic University,*
*Polytechnicheskaya Str., 29, Saint-Petersburg, 195251, Russia*
*Tel/fax: +7-812-552-6621, e-mail: aerofmf@citadel.stu.neva.ru*

Turbulent Rayleigh-Bénard (RB) convection in mercury ($Pr = 0.025$) and water ($Pr = 7$) at high Rayleigh numbers is numerically studied using a hybrid RANS/LES (Reynolds-Averaged Navier-Stokes / Large Eddy Simulation) approach, developed in the context of the Detached Eddy Simulation (DES) idea. Turbulence modelling is based on the one-equation model for the kinetic energy of unresolved motion. The computations have been performed for a cubic cell (filled with water) and for a cylindrical cell (filled with mercury) of aspect ratio 1 at the Rayleigh number ranging from $10^8$ to $5\times10^9$. Results of computations are described in comparison with known experimental data, in particular, for thermal and viscous boundary layer thicknesses. The specific patterns of fully developed turbulent convection are clearly indicated, especially the formation of a large-scale circulation cell and thermal plumes for both the configurations. Numerically predicted Nusselt numbers are in quantitative agreement with registered experimental laws.

## I. INTRODUCTION

The colossal progress in computer performance and memory has made wide-ranging numerical studies of turbulent natural convection flows on the base of 3D unsteady formulation possible [1]. *Direct Numerical Simulation* (DNS) is the most attractive and reliable approach to get a detailed knowledge of convection [2 - 4]. However, full resolved DNS remains to be extremely time-consuming for Rayleigh numbers exceeding $10^7$. Many recent contributions are devoted to applications of *Large Eddy Simulation* (LES) that can be used at much higher Rayleigh numbers than DNS. In case of LES applications to wall-bounded flows the major difficulties are associated with the treatment of the near-wall layers [e.g., 5]. Recent works propose hybrid techniques combining RANS (*Reynolds-Averaged Navier-Stokes*) and LES approaches to use their advantages in the appropriate flow regions [6, 7]. One of these techniques is the *Detached Eddy Simulation* (DES) [6]. Considering impressive achievements in DES of massively separated flows [8], it is of certain interest to extend fields of DES application for prediction of turbulent thermal convection at high Rayleigh numbers. Remarkably that there is a similarity between the massively separated flows and the buoyant flows under highly unstable conditions in the sense that the interaction of large eddies occupying the flow core with thin boundary layers on confining walls play the dominant role in the turbulent transport.

Rayleigh-Bénard (RB) convection is intensively investigated both experimentally and numerically [9]. Most of numerical simulations of high-*Ra* RB convection were performed in domains of large aspect ratio for test fluids with $Pr \sim 1$ [2, 5, 10]. Numerical information on turbulent RB convection in enclosures with aspect ratio of order 1 is extremely limited [11].

The present work is aimed at numerical simulation of strongly turbulent RB convection in confined enclosures of aspect ratio 1 for Rayleigh numbers up to $5\times10^9$. Mercury and water, characterized by essentially different Prandtl numbers, have been chosen as test fluids. Turbulence modelling is performed with a DES-like technique involving the equation of the kinetic energy of unresolved motion. Results of computations are presented in comparison with experimental data.

## II. PROBLEM DESCRIPTION

The problem under consideration is thermal convection in confined cubic and cylindrical cells of aspect ratio 1 heated from below. The cell height $H$ is taken as a length scale. The cold top and hot bottom plates are maintained at constant temperature ($T_h$ and $T_c$ respectively), the gravity vector, $\boldsymbol{g}$, points downwards. The temperature difference $\Delta T = T_h - T_c$ is used to introduce normalised temperature, $\Theta = (T - T_c)/\Delta T$. The lateral walls of the cells are adiabatic. No-slip velocity boundary conditions are imposed on all the walls. The buoyancy velocity, $V_b = (g\beta\Delta TH)^{1/2}$, is taken as a velocity scale, and the ratio $H/V_b$

serves as a time scale. With given geometry, the flow dynamics in the cells is determined by two non-dimensional parameters: the Prandtl number, $Pr = \nu/a$, and the Rayleigh number, $Ra = g\beta\Delta TH^3/(\nu a)$. Below turbulent regimes of RB mercury convection ($Pr = 0.025$) are considered for a cylindrical cell, and turbulent water convection at $Pr = 7$ is studied for a cubic cell.

## III. GOVERNING EQUATIONS AND TURBULENCE MODELLING

With the Boussinesq approximation for incorporation of buoyancy effects, the governing equations for resolved components of time-dependent velocity and temperature fields can be written in a non-dimensional form as follows

$$\nabla \cdot \boldsymbol{V} = 0 \tag{1}$$

$$\frac{d\boldsymbol{V}}{dt} = -\nabla p^* + Div\left(2\nu_{eff}\,\dot{\boldsymbol{S}}\right) + \Theta \boldsymbol{e}_z \tag{2}$$

$$\frac{d\Theta}{dt} = \nabla \cdot \left(a_{eff} \nabla \Theta\right). \tag{3}$$

Here $p^*$ is the reduced pressure, $\boldsymbol{e}_z$ is the unity vector of vertical coordinate $z$, $\dot{\boldsymbol{S}}$ is the resolved strain-rate tensor, $\nu_{eff} = \sqrt{Pr/Ra} + \nu_t$ is the non-dimensional effective viscosity, $\nu_t$ is the eddy viscosity given by a model of unresolved turbulence, $a_{eff} = 1/\sqrt{Ra \cdot Pr} + \nu_t / Pr_t$, and $Pr_t$ is the subscale turbulent Prandtl number.

The effects of unresolved scales are taken into account using the RANS/LES hybridization. In the framework of the eddy viscosity concept, equations (1) to (3) for the RANS region formally look identical to those written for LES. The difference consists in the meaning of the eddy viscosity. In the near-wall layers (RANS region) the eddy viscosity has to reflect the effect of "all-scales" turbulence whereas in the off-wall flow part (LES region) its role is attributed to the subgrid-scale turbulence.

The DES-like one-equation $k$-transport model used in the present computations is formulated as follows [12]. The governing equation for the unresolved-motion kinetic energy, $k$, can be written as

$$\frac{\partial k}{\partial t} + \nabla \cdot (\boldsymbol{V}\, k) = \nabla \cdot \left(\nu_{eff} \nabla k\right) + 2\nu_t \dot{\boldsymbol{S}}^2 - \bar{\varepsilon}. \tag{4}$$

RANS/LES region switching is controlled via comparison of dissipation rates given by the RANS model and the subgrid-scale model of LES

$$\bar{\varepsilon} = max\left\{\varepsilon^{RANS}, \varepsilon^{LES}\right\}, \tag{5}$$

where $\varepsilon^{LES}$ is given by $\varepsilon^{LES} = C_\varepsilon k^{3/2} / \Delta$, and $\Delta = \left(\Delta_1 \Delta_2 \Delta_3\right)^{1/3}$ is the volume of the grid cell. To define $\varepsilon^{RANS}$, relations of the low-*Re* RANS model developed by Wolfshtein [13] are used

$$\varepsilon^{RANS} = k^{3/2} \Big/ \left(l \cdot F_\varepsilon\right),\ l = \kappa\, C_\mu^{-3/4} y,\ F_\varepsilon = 1 - exp\left(-\, Re_y / A_\varepsilon\right),\ Re_y = \sqrt{k}\, y / \nu,\ \kappa = 0.41. \tag{6}$$

Here $y$ is the distance to the nearest wall, and $F_\varepsilon$ is the factor introduced to increase properly the dissipation rate near the wall. The eddy viscosity is calculated as

$$\nu_t = C_\mu\, f_\mu\left(Re_t\right) l_t \sqrt{k},\ \ Re_t = \sqrt{k}\, l_t / \nu,\ \ l_t \equiv k^{3/2} / \bar{\varepsilon}. \tag{7}$$

The damping factor that can be used in the RANS region of the hybrid solution is

$$f_\mu = 1 - exp\left(-\, Re_y / A_\mu\right). \tag{8}$$

To provide a continuous variation of the eddy viscosity near the interface between the LES and RANS regions, it is reasonable to write $f_\mu$ for the LES region as

$$f_\mu = 1 - exp\left[-\, Re_t \Big/ \left(A_\mu \kappa C_\mu^{-3/4} F_\varepsilon\left(Re_y\right)\right)\right] \quad . \tag{9}$$

Model constants are $Pr_t = 0.4$, $C_\varepsilon = 0.75$, $C_\mu = 0.09$, $A_\mu = 10$, $A_\varepsilon = 5.1$.

## IV. COMPUTATIONAL ASPECTS

Computations in the framework of the above formulation have been carried out using a well-validated in-house code (named SINF). This advanced 3D Navier-Stokes solver is based on the second-order finite-volume spatial discretisation using the cell-centred variable arrangement and body-fitted block-structured grids. The discretisation of time derivatives is done with a three-time-level, second-order implicit scheme. The artificial-compressibility method is applied at each time step. The code is in wide use for solving both fundamental and industrial problems. Additional details of the solver can be found elsewhere [14].

The cylindrical cell was covered by a two-block grid and the cubic cell was covered by a single-block grid both consisting of about 160,000 cells, with nodes clustered to all the walls so that the normalised time-averaged near-wall coordinate for the first computational point, $y^+$, was less than unity. As a result of preliminary study, the non-dimensional time step was set to 0.1. The computations for the first run for both the configurations were started from zero velocity and $\Theta = 0.5$ temperature fields. After a transient period of 100 time units, a statistically developed regime was obtained. For the other runs, the computations were started from an instantaneous field saved for the first case and transient periods of about 50 time units were passed. Samples computed after transient periods were next to 200 - 300 time units.

## V. RESULTS AND DISCUSSION

### *1. Structure of turbulent convection*

The present computations of mercury convection have been performed for the Rayleigh number ranging from $10^8$ to $5\times10^9$, and the water convection has been simulated at $Ra = 5\times10^8$ and $5\times10^9$.

For both the cells the computed convection is characterised by formation of a stable large-scale circulation that spans the height of the cell. This result is in accordance with experimental observations [15, 16]. The presence of the global circulation in the cubic enclosure is illustrated in Fig. 1 ($Ra = 5\times10^9$). It can be seen that two equiscalar surfaces of vertical velocity corresponding to the absolute value of 0.05 are mostly located on different sides with respect to a cubic diagonal plane. Despite some disorder attributed to chaotic motion components, the global structure detected keeps the individuality for all the convection regimes considered. In principal, in case of the cubic cell four variants of the large-scale structure are possible (two directions of fluid circulation by two cubic diagonal planes). In the present computations, the selection of the orientation/direction of the global circulation was due to uncontrolled numerical reasons (non-symmetry in the numerical algorithm, rounding of numbers, etc). In case of the cylindrical cell the global structure slowly changed its orientation in time that could be quite expected due to the axial symmetry of the cell.

Quantitatively the global circulation can be characterized by the maximum horizontal temperature difference, $\Delta\Theta_h$, and by the maximum vertical velocity difference, $\Delta w_h$, both evaluated at the mid-plane. The present RANS/LES has resulted in $\Delta\Theta_h$ and $\Delta w_h$ that are about three times larger for mercury than for water, i.e., the global circulation in mercury is of considerably higher intensity at a fixed $Ra$.

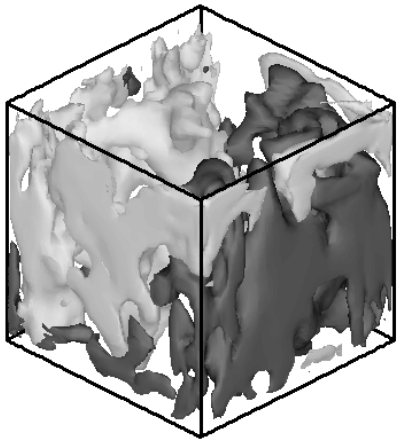

*Fig. 1. Equiscalar surfaces of vertical velocity w=0.05 (black) and w=-0.05 (gray): $Ra=5\times10^9$, Pr=7.*

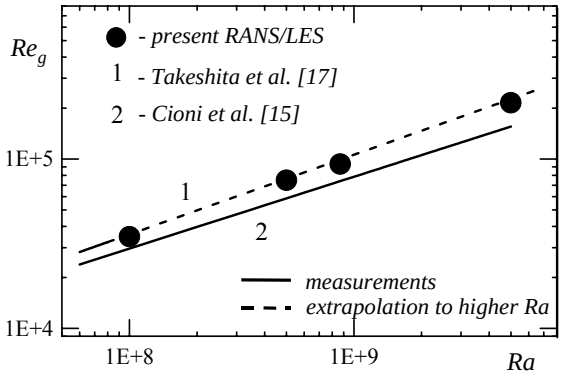


*Fig. 2. Reynolds vs Rayleigh numbers for mercury in comparison with experimental data.*

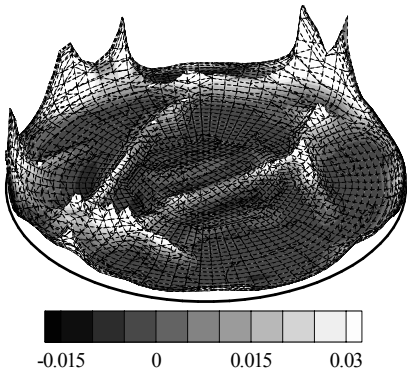


*Fig. 3. Temperature isosurface $\Theta = 0.9$ colored by vertical velocity. Mercury, $Ra = 5\times10^8$.*

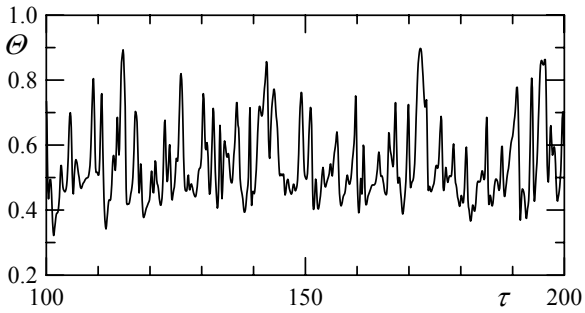


*Fig. 4. Temperature fluctuations near the bottom plate ($z = 0.03$, $r = 0$). Mercury, $Ra = 5\times10^8$.*

The $\Delta\Theta_h$ and $\Delta w_h$ values decrease with increasing the Rayleigh number in the *Ra*-range covered by present work for both the fluids. For mercury, this decrease could be approximated by the factor of $Ra^{-0.05}$. Note that DNS results [11] indicated the $\Delta\Theta_h$ and $\Delta w_h$ independence from *Ra* for moderate $Ra \le 10^6$. This observation was reproduced in our test computations of mercury convection at $Ra \le 10^6$ as well.

Following [11], we introduce a scale velocity of the global circulation, $V_g$, determined as a half of the $\Delta w_h$, the latter is extracted from the computed data directly. For mercury convection, the corresponding Reynolds number, $Re_g = V_g \cdot H / \nu$, *versus* the Rayleigh number is shown in Fig. 2. The computed values of $Re_g$ are in a good agreement with scaling laws obtained in the experiments [15, 17]. It should be noted, however, that experimental values of $V_g$ were obtained indirectly using information about the peak frequency of the temperature spectra.

Analyzing time-dependent flow field patterns one is able to follow coherent thermal plumes arising from the top and bottom temperature boundary layers for both the configurations. These plumes are quite intensive in water convection that is in accordance with experimental data [16, 18]. In mercury thermal plumes are noticeably weaker. The reason for the plume weakness in mercury could be attributed to a larger thermal diffusivity that suppresses the vertical detachment of fluid portions [11, 17]. Note that the thermal plumes activity has not been indicated previously both in numerical [11] and experimental [15, 17] studies of mercury convection. In the present RANS/LES computations the plumes were detected via observation of instantaneous temperature field in the vicinity of the isothermal walls, as it is illustrated in Fig. 3 for the near-bottom region. As well, sharp one-way peaks in temperature fluctuations near the outer edge of the thermal boundary layer visible in Fig. 4 may be associated with the thermal plumes. Thus, for high-*Ra* mercury convection, thermal plumes affect the global circulation and lead to smoothing of horizontal inhomogeneity of temperature field.

Strong turbulent mixing at high *Ra* leads to formation of thin high-gradient boundary layers near the isothermal walls. In turn, the global circulation affects viscous boundary layers. In the present work, following [11, 18], the viscous boundary layer thickness, $\delta_V$, and the thermal boundary layer thickness, $\delta_T$, were estimated taking the position at which the extrapolation of the linear part of the time-averaged horizontal velocity (temperature) profile achieves the maximum horizontal velocity (the mean temperature at

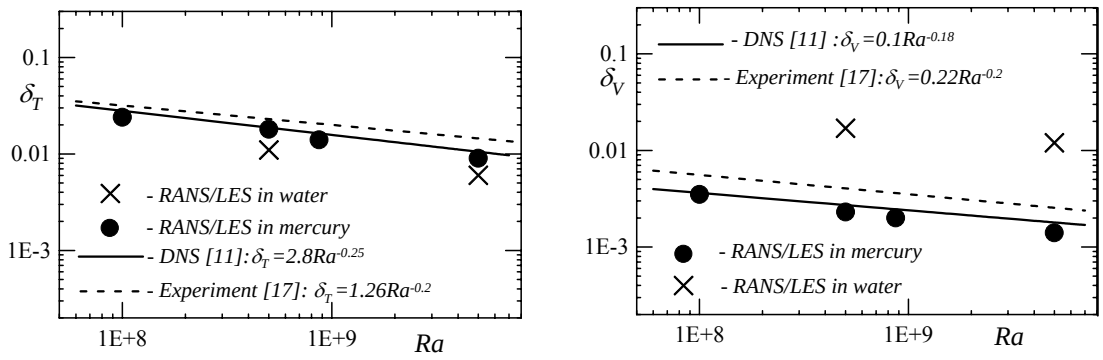


*Fig. 5. Thermal (left) and viscous (right) boundary layer thicknesses as functions of the Rayleigh number. Comparison with extrapolations of experimental and DNS data for mercury to higher Ra.*

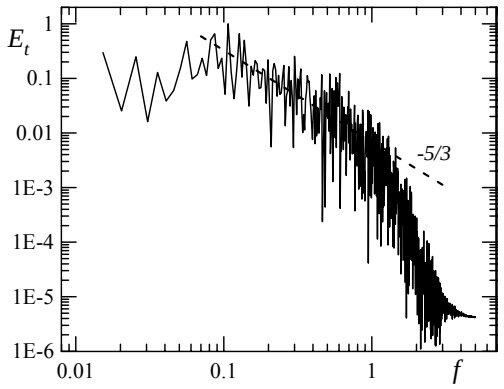


*Fig. 6. Power spectral density of temperature fluctuations ($z = 0.25$, $r = 0$). Mercury, $Ra = 5\times10^8$.*

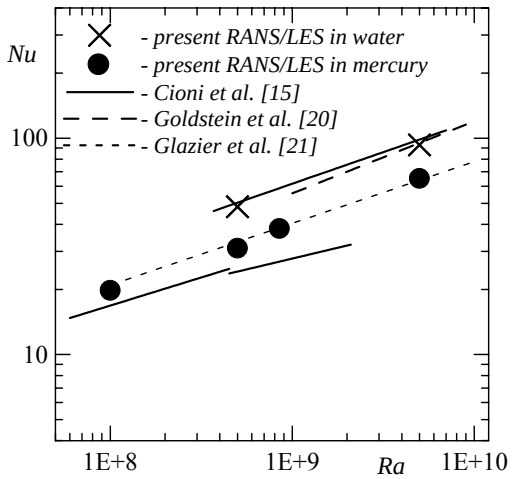


*Fig. 7. Nusselt vs Rayleigh numbers in comparison with experimental data.*

the mid-plane). Data on $\delta_T$ and $\delta_V$ obtained from the profiles taken at the central axis of the cell are given in Fig. 5. For mercury, the computed values of $\delta_T$ and $\delta_V$ agree well with the power law fits also shown in the Figure. These fits are extrapolations of the experimental and DNS data presented in [11, 17]. The Prandtl number effect appears in the $\delta_T$ to $\delta_V$ ratio. For the mercury case, the viscous layer is nested within the thermal boundary layer. Results for water (daggers in Fig. 5) point to a reverse relation between $\delta_T$ and $\delta_V$, i.e., the thermal boundary layer is considerably thinner than the viscous one.

An examination of scaling laws in mercury temperature fluctuations spectra is presented in Fig. 6. The spectrum computed for a point located away from the walls shows a scaling law that is close to the Kolmogorov "5/3" law. This result being in accordance with the previous experimental findings [19] indicates that in low-*Pr* convection temperature behaves as a passive scalar in the regions away from the walls. The spectrum computed for water differs from that computed for mercury and has an extended range of decreasing with the "7/5" law.

## *2. Heat transfer predictions*

The above discussed prominent features of turbulent RB convection determine the heat transport across the cell, and the global circulation and thermal plumes contributions to heat transfer change with varying Prandtl numbers. At moderate *Ra* in mercury the heat is mostly transported by the global circulation along the cell boundaries [11, 17]. However, as mentioned above, in strong turbulent regimes, $Ra > 10^8$, an increase in the Rayleigh number is accompanied by a decrease in the global circulation intensity. Consequently, the thermal plumes start to be formed in the convective flow and to take the role of an additional heat carrier. In the water convection the heat is mainly transported by the thermal plumes, and the role of the global circulation is less significant [18].

Fig. 7 shows that the Nusselt numbers computed are in quantitative agreement with known experimental laws for both the fluids [15, 20, 21]. However, a notable difference in the *Nu* values measured for mercury at similar configurations is visible [15, 21] that can be attributed to difficulties in controlling the low-*Pr* fluid experiments. The present RANS/LES results obtained for mercury are very close to a fit from [21] giving $Nu \propto Ra^{0.285}$ over a wide range of *Ra*, up to $8\times10^{10}$.

Several recent experiments at very high *Ra* values point to appearance of a new "ultrahard" regime, characterized by more efficient heat transport as compared with "hard" turbulence regime [15, 22]. In particular, for gaseous helium an increasing scaling exponent was registered above $Ra \approx 10^{11}$ [22]. In mercury, the transition to a new regime was found at $Ra > 2\times10^9$ [15]. However, these observations are balanced by other experiments showing no transition to any "ultrahard" regime at similar *Ra* [21]. The present computations of the mercury convection at *Ra* up to $5\times10^9$ do not indicate any increase in the power law for the Nusselt number.

## VI. CONCLUSIONS

A hybrid RANS/LES technique has been successfully applied to study the high-*Ra* Rayleigh-Bénard convection in cells of aspect ratio 1 filled with mercury (cylindrical cell) or water (cubic cell). The Rayleigh number was ranged from $10^8$ to $5\times10^9$.

The development of a large-scale circulation was observed in numerical solutions, in accordance with previous experimental findings. In mercury the global circulation is considerably more intensive than in water. For both the fluids the circulation intensity weakens with an increase in *Ra* that is attributed to intensification of thermal plumes. A scale velocity of the global circulation computed for mercury agree well with known experimental data.

A dependence of thermal and viscous boundary layers thicknesses on the Rayleigh number has been established and compared with literature data known for lower *Ra*.

A comparison of computed Nusselt numbers with measured data has shown a good agreement with experimental laws for both the fluids. No transition to a "ultrahard" regime reported in some experimental studies of mercury convection was observed in the present computations.

## ACKNOWLEDGEMENTS

The study has been supported by the Russian Foundation of Basic Research, grant 01-02-16697.

## REFERENCES

1. Smirnov, E.M. Recent advances in numerical simulation of 3D unsteady convection controlled by buoyancy and rotation, CD-ROM Proc. of the 12th International Heat Transfer Conference, Grenoble, France (2002) 12p.
2. Julien, K., Legg S., McWilliams J., and Werne J. Rapidly rotating turbulent Rayleigh-Bénard convection, J. Fluid Mech. 322 (1996) 243-273.
3. Kerr, M.R. Rayleigh number scaling in numerical convection, J. Fluid Mech. 310 (1996) 139-179.
4. Kerr, M.R., and Herring, J.R. Prandtl number dependence of Nusselt number in DNS, J. Fluid Mech. 419 (2000) 325-344.
5. Kimmel, S.J., and Domaradzki, J.A. Large eddy simulations of Rayleigh-Bénard convection using subgrid scale estimation model, Phys. Fluids 12 (2000) 169-184.
6. Spalart, P.R., Strategies for turbulence modelling and simulations, Int. J. Heat and Fluid Flow. 21 (2000) 252-263.
7. Speziale, C.G. Turbulence modeling for time-dependent RANS and VLES: a review, AIAA J. 36 (1998) 173-184.
8. Strelets, M. Detached eddy simulation of massively separated flows, AIAA Paper 2001-0879 (2001) 18p.
9. Siggia, E.D. High Rayleigh number convection, Annu. Rev. Fluid Mech. 26 (1994) 137-168.
10. Kenjereš, S., and Hanjalić, K. Transient analysis of Rayleigh-Bénard convection with a RANS model, Int. J. Heat and Fluid Flow 20 (1999) 329-340.
11. Verzicco, R., and Camussi, R. Prandtl number effects in convective turbulence, J. Fluid. Mech. 383 (1999) 55-73.
12. Abramov, A.G., and Smirnov, E.M. Numerical study of strongly turbulent Rayleigh-Bénard convection in mercury with a hybrid RANS/LES approach, (2002) (submitted for publication).
13. Wolfshtein, M. The velocity and temperature distribution in one-dimensional flow with turbulence augmentation and pressure gradient, Int. J. Heat and Mass Transfer 12 (1969) 301-318.
14. Smirnov, E.M., Solving the full Navier-Stokes equations for very-long-duct flows using the artificial compressibility method, CD-ROM Proc. of the ECCOMAS 2000 Conf., Barcelona, Spain (2000) 17p.
15. Cioni, S., Ciliberto, S., and Sommeria, J. Strongly turbulent Rayleigh-Bénard convection in mercury: comparison with results at moderate Prandtl number, J. Fluid Mech. 335 (1997) 111-140.
16. Zocchi, G., Moses, E., and Libchaber, A. Coherent structures in turbulent convection, an experimental study, Physica A. 166 (1990) 387-407.
17. Takeshita, T., Segawa, T., Glazier, J.A., and Sano, M. Thermal turbulence in mercury, Phys. Rev. Lett. 76 (1996) 1465-1468.
18. Belmonte A., Tilgner, A., and Libchaber, A. Temperature and velocity boundary layers in turbulent convection, Phys. Rev. E. 50 (1994) 269-279.
19. Cioni S., Ciliberto S., and Sommeria, J. Experimental study of high-Rayleigh-number convection in mercury and water, Dynamics of Atmospheres and Oceans 24 (1996) 117-127.
20. Goldstein, R.J., and Tokuda, S. Heat transfer by thermal convection at high Rayleigh numbers, Int. J. Heat Mass Transfer. 23 (1980) 738-740.
21. Glazier, J.A., Segawa, T., Naert, A., and Sano, M. Evidence against 'ultrahard' thermal turbulence at very high Rayleigh numbers, Nature 398 (1999) 307-310.
22. Chavanne, X., Chilla, F., Castaing, B., and Hébral, D. Turbulent Rayleigh-Bénard convection in gaseous and liquid He, Phys. Fluids 13 (2001) 1300-1320.